Optimal Preview Control of a Dual-Stage Actuator System for Triangular Reference Tracking

Li Wang, Jinchuan Zheng, *Member, IEEE*, and Minyue Fu, *Fellow, IEEE*

***Abstract*— This brief proposes an optimal preview control law for a dual-stage actuator (DSA) system to track triangular reference, which is essential in many raster scan motion control applications. The main difficulty of tracking triangular reference is to follow the waveform fast and accurately when its slope switches. For this goal, we first discuss a time-optimal controller (TOC) for the primary stage, which is a double integrator system. The TOC is then proved to achieve the minimum overshoot. This result is a new contribution to DSA control applications because it leads to a reference profile of minimum amplitude for the secondary stage to follow and thus significantly prevents the saturation of the secondary actuator. Subsequently, we propose an optimal preview control with the use of the information of the future reference to further reduce the settling time and overshoot. Finally, the secondary actuator controller is also given. Experimental results are shown to verify the effectiveness of the proposed control design.**

***Index Terms*— Actuator saturation, dual-stage actuator (DSA), motion control, preview control.**

I. Introduction

DUAL-STAGE actuator (DSA) servomechanisms are typically characterized by a structural design with two actuators connected in series along a common axis. The primary actuator (coarse actuator) possesses a long travel range but with poor accuracy and slow response. The secondary actuator (fine actuator) is typical of higher precision and faster response but with a limited travel range. By combining the DSA system with properly designed servo controllers, the two actuators are complementary to each other and the defects of one actuator can be compensated by the merits of the other one. Therefore, the DSA system can provide large travel range, high positioning accuracy and fast response. The DSA servomechanisms have attracted considerable industrial application such as the dual-stage hard disk drive actuator [1]–[3], the dual-stage machine tools [4], macro/micro robot manipulators [5], [6], and the dual-stage XY positioning tables [7].

Manuscript received September 22, 2013; revised January 12, 2014; accepted January 16, 2014. Manuscript received in final form January 19, 2014. Date of publication February 6, 2014; date of current version October 15, 2014. This work was supported by the NSFC under Grant 61134001. Recommended by Associate Editor T. Parisini.

L. Wang is with the School of Control Science and Engineering, Zhejiang University, Hangzhou 310058, China (e-mail: li.wangzju@gmail.com).

J. Zheng is with the School of Software and Electrical Engineering, Swinburne University of Technology, Hawthorn VIC 3122, Australia (e-mail: jzheng@swin.edu.au).

M. Fu is with the School of Electrical Engineering and Computer Science, The University of Newcastle, Callaghan NSW 2308, Australia, and also with the Zhejiang University, Hangzhou 310058, China (e-mail: minyue.fu@newcastle.edu.au).

Color versions of one or more of the figures in this paper are available online at http://ieeexplore.ieee.org.

Digital Object Identifier 10.1109/TCST.2014.2301823

The mechanical design of DSA systems appears to be simple, but the control of the DSA systems is not straightforward because of several reasons. First, the DSA system contains two control inputs but only one control output, which requires a proper control strategy for control allocations of the two actuators in response to a reference input. Second, the actuators have input constraints in practice, which results in difficulties when actuator saturation occurs. As such, these specific characteristics have raised challenging tasks for DSA control design to yield an optimal performance. A variety of approaches have been reported to deal with the dual-stage control problems. For example, the control design for track following and settling (i.e., disturbance and residual vibration rejection control problem) can be found in [8]–[10]. The secondary actuator saturation problem was explicitly considered during the control design [11]–[13]. Tracking control is another main control task to drive the position output to track a desired trajectory such as setpoint references, which is used to perform pick-and-place operations in nanoassembly [14] and power sintering process [15]. Moreover, triangular reference is the most common trajectories used in scanning probe devices, which typically combine a triangular waveform in the x-axis and a linear ramp in the y-axis to achieve the desired raster scan motion [16], [17]. Though the setpoint tracking control has been extensively discussed [18], [19], triangular reference tracking control is rarely studied in the literature. Therefore, this brief is focused on the control of DSA systems for triangular reference tracking with fast and accurate performance.

Because of the redundancy of actuators, the dual-stage control design is divided into two control problems, one for each stage. The primary stage control problem is to enable the primary actuator to track the triangular reference in minimal time when the slope changes, whilst allowing the tracking error within a manifold, which thus motivates the preview control. The secondary-stage control problem is then to make the secondary actuator compensate for the tracking error produced by the primary actuator, which if achieved can lead to accurate tracking of the triangular reference. Note that the control design for the two stages is closely related because the primary-stage tracking error needs to be guaranteed within the secondary actuator's travel range. Conversely, the secondary-stage control needs to incorporate the primary-stage's state to achieve sufficient compensation of the primary-stage tracking error.

There has been a lot of research on preview control. For example, [20] applied preview control to stable inversion of nonlinear nonminimum-phase systems. Discrete-time H_∞ preview control can be found in [21]. Our contribution in

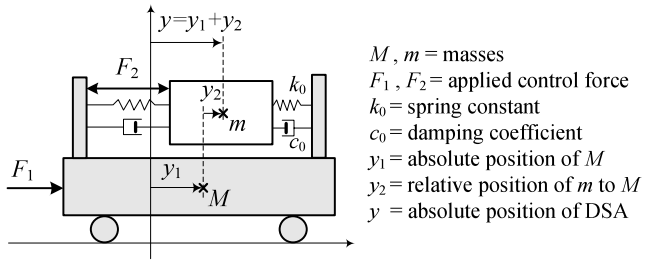

Fig. 1. Illustration of a class of DSA model.

this brief lies in the new optimal preview control for the primary actuator. In particular, we develop a nonpreview time optimal controller (TOC) and an optimal preview controller. It is proved that these controllers have the properties of both time optimal and minimal tracking error performance. Our preview control differs from the conventional preview control [22], which uses the augmented system with the preview information to generate the preview feedforward control input that may require a large computational load. In our work, we give the optimal control law directly for the continuous time system and the result has a simple explicit expression without solving a complex optimization problem. Another advantage of our work is that we give an explicit expression of the required preview time. For the secondary actuator control design, we simply employ a feedback-feedforward controller modified based upon the method we previously reported. As such, the combined dual-stage controller is shown to achieve fast and accurate tracking of triangular references as verified by experimental results. The control law proposed in this brief is based on the condition that the positions of both the primary and the secondary actuator are measurable. This may not be applicable to some applications such as hard disk drives, where only the total position output is measurable. In this case, a state estimator could be designed prior to applying the proposed control law, the performance of which, however, is yet investigated in this brief.

The rest of this brief is organized as follows. Section II presents the DSA model and formulates the dual-stage control problems. Section III derives the solution for the primary-stage control, which includes a nonpreview TOC and an optimal preview controller. Section IV simply gives the controller design for the secondary actuator. Section V shows the experimental results of the proposed control to validate its effectiveness. Finally, concluded remarks are given in Section VI.

II. Problem Formulation

We consider a class of DSA system that can be shown by Fig. 1, where M and m denote the mass of the primary and secondary stages, respectively, F_1 and F_2 the actuator applied control force, and y the total position output of the DSA. During the process of mechanism design, it is typical to select the configurations of two stages such that $M \gg m$, $|y_1| \gg |y_2|$, and $|F_2/F_1| \gg m/M$. In this way, the coupling forces between the two actuators can be simply ignored and the dynamic equations of the DSA system are given by

$$\begin{cases} M\ddot{y}_1 = F_1 \\ m\ddot{y}_2 = F_2 - c_0\dot{y}_2 - k_0 y_2. \end{cases} \tag{1}$$

A typical experimental setup that matches the model in Fig. 1 has been reported in [19] (see also Fig. 6), where the primary stage is driven by a linear motor (LM) and the secondary stage by a piezo actuator (PA). Suppose the power amplifier gain of each actuator is g_1 and g_2, respectively, and substitute $F_i = g_i u_i$ $(i = 1, 2)$ to (1), where u_i is the actuator control input. We can easily obtain the state-space model for the DSA system as follows:

$$\begin{cases} \Sigma_1 : \dot{x}_1 = A_1 x_1 + B_1 u_1 \\ \Sigma_2 : \dot{x}_2 = A_2 x_2 + B_2 u_2 \\ y = y_1 + y_2 = C_1 x_1 + C_2 x_2 \end{cases} \tag{2}$$

where the state $x_1 = [y_1 \;\; \dot{y}_1]^T$, $x_2 = [y_2 \;\; \dot{y}_2]^T$, and

$$A_1 = \begin{bmatrix} 0 & 1 \\ 0 & 0 \end{bmatrix}, \quad B_1 = \begin{bmatrix} 0 \\ b_1 \end{bmatrix}, \quad C_1 = \begin{bmatrix} 1 & 0 \end{bmatrix}$$
$$A_2 = \begin{bmatrix} 0 & 1 \\ a_1 & a_2 \end{bmatrix}, \quad B_2 = \begin{bmatrix} 0 \\ b_2 \end{bmatrix}, \quad C_2 = \begin{bmatrix} 1 & 0 \end{bmatrix}$$

with $b_1 = g_1/M$, $a_1 = -k_0/m$, $a_2 = -c_0/m$, and $b_2 = g_2/m$. Moreover, the control inputs of the two actuators and the secondary actuator output have the constraints

$$|u_1| \le \bar{u}_1, \quad |u_2| \le \bar{u}_2, \quad |y_2| \le \bar{y}_2 \tag{3}$$

where $\bar{u}_1$ and $\bar{u}_2$ denote the maximum control input of the actuator, respectively, and $\bar{y}_2$ is the maximum travel range of the secondary actuator.

For the DSA system in (2), our control objective is to design the control law u_1 and u_2 such that the total DSA output can track a triangular reference $r(t)$ fast and accurately. An intuitive control strategy is to design u_1 to drive the primary actuator to track the reference at its best capability; and then u_2 is designed to drive the secondary actuator to compensate the residual tracking error of the primary actuator. Provided that the tracking error is within the secondary actuator's travel range and the secondary actuator has a much faster dynamics, the resulting total tracking error of the DSA will be negligible. In general, the control difficulty occurs when the slope of the triangular reference changes because the primary stage typically suffers from an overshoot and requests a tedious time to settle down to steady state. Therefore, in the sequel, we will focus on how to design u_1 to reduce the transition time and the overshoot. Moreover, we propose a preview control method if the further information of the reference is known in advance. Fig. 2 shows the preview control strategy, where 0 is the switching time instant at which the slope of the triangular reference changes; τ_p is the preview time; and τ_s is the settling time. We assume that the period of the reference is sufficiently long so that the tracking error will be able to reach zero before the waveform switches direction. Furthermore, we have the following definitions.

1) The tracking error of the primary stage is denoted by

$$e_1(t) := y_1(t) - r(t). \tag{4}$$

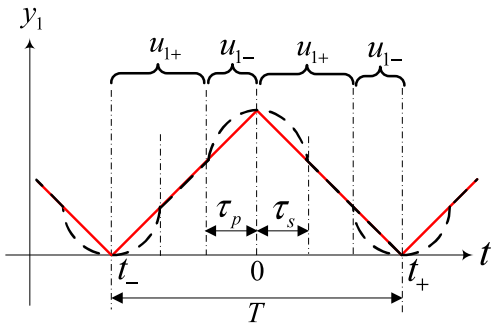

Fig. 2. Illustration of preview control strategy for the primary actuator. Solid line: triangular reference $r(t)$. Dashed line: output response of the primary actuator $y_1(t)$ with preactuation. We set the time $t = 0$ to represent the switching time instant at which the slope of the triangular reference switches; τ_p the preview time; τ_s the settling time; and T the period of the triangular reference. u_{1-} represents the preview control input and u_{1+} represents the post-actuation control input; and the brackets underneath represent the time zones that the control inputs apply to.

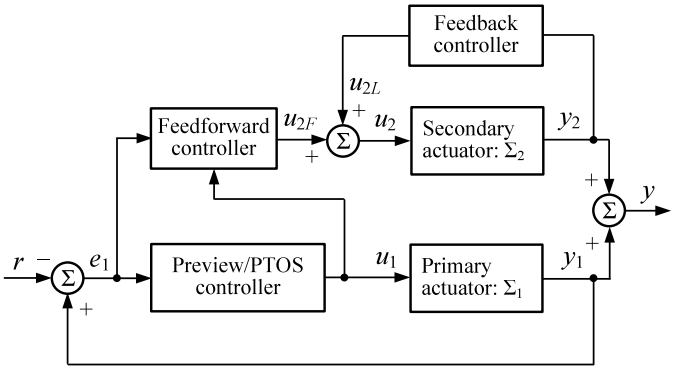

Fig. 3. Block diagram of the DSA control structure.

Here, the triangular reference $r(t)$ has the characteristics that $\dot{r}(t)$ and $\ddot{r}(t)$ are both piecewise constant but have a discontinuity when the slope of the triangular reference switches.

2) The overshoot denotes the maximum tracking error

$$\text{overshoot} := \max |e_1(t)|. \tag{5}$$

3) The minimum overshoot is denoted by σ, which is defined by

$$\sigma := \min_{u_1 \in \mathcal{U}} \max |e_1(t)| \tag{6}$$

where $\mathcal{U}$ represents the set of all feasible control inputs.

The block diagram of the DSA control structure is shown in Fig. 3. In the following, we will formulate the control problem for each actuator, respectively.

A. Primary Actuator Control Problem

For a given triangular reference $r(t)$, find a controller

$$u_1(t) = \begin{cases} u_{1-}(t), & -\tau_p \le t \le 0 \\ u_{1+}(t), & t > 0 \end{cases} \tag{7}$$

subjected to

$$|u_1(t)| \le \bar{u}_1 \tag{8}$$

and an appropriate preview time $\tau_p \ge 0$ such that

$$\sigma \text{ is achieved.} \tag{9}$$

Based on (9), there are two other goals

$$\tau_s \text{ is minimized} \tag{10}$$

$$\tau_p \text{ is minimized.} \tag{11}$$

If such an u_1 exists, we call it an optimal preview control. Moreover, if we choose $\tau_p = 0$ where no preview control is applied, then the resulting controller is called nonpreview time-optimal control.

B. Secondary Actuator Control Problem

Given the designed primary actuator controller, find a controller

$$|u_2(t)| \le \bar{u}_2 \tag{12}$$

such that the secondary actuator output y_2 can compensate for the tracking error generated by the primary actuator, i.e., $y_2 \approx -e_1$. Thus, we can achieve

$$y = y_1 + y_2 = e_1 + r + y_2 \approx r \tag{13}$$

which implies that the total DSA output can track the triangular reference accurately.

III. Primary Actuator Control Design

This section addresses the solution to the primary actuator control problem, as stated in Section II-A. We first derive a time-optimal control law without preview, based upon which an optimal preview control law is proposed. Finally, a proximate time-optimal servomechanism (PTOS) controller is combined with the proposed control law to achieve robust tracking performance.

A. Nonpreview Time-Optimal Control

We first transform the primary actuator system into the error space in the following form:

$$\dot{x}_e = \underbrace{\begin{bmatrix} 0 & 1 \\ 0 & 0 \end{bmatrix}}_{A_e} x_e + \underbrace{\begin{bmatrix} 0 \\ b_1 \end{bmatrix}}_{B_e} u_1 \tag{14}$$

where $x_e = [e_1 \;\; \dot{e}_1]^T$, $|u_1| \le \bar{u}_1$, and the initial state of the system is given by

$$x_e(0) = [e_1(0) \;\; \dot{e}_1(0)]^T. \tag{15}$$

Firstly, we aim to find a TOC $u_1(t)$, $t \ge 0$ for (14) to achieve the goal of (10) for any initial state $x_e(0)$. It is well known that the solution is a bang-bang function [23], whose control law is directly given by

$$u_1^*(t) = \text{sign}^\dagger\left(-\text{sign}(e_1(t))\sqrt{2b_1\bar{u}_1|e_1(t)|} - \dot{e}_1(t), -\dot{e}_1(t)\right)\bar{u}_1 \tag{16}$$

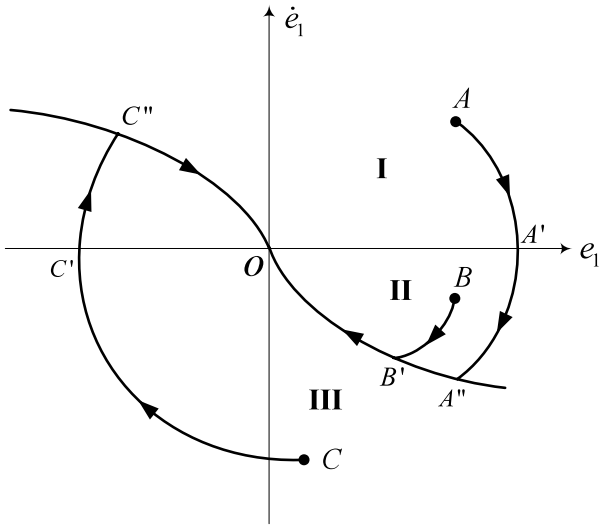

Fig. 4. System state trajectory under the time-optimal control law, which is shown to be optimal control law for minimum overshoot as well.

where $\text{sign}(\cdot)$ and $\text{sign}^{\dagger}(\cdot,\cdot)$ are defined as follows:

$$\text{sign}(\Omega) = \begin{cases} +1, & \Omega > 0 \\ -1, & \Omega < 0 \\ 0, & \Omega = 0 \end{cases} \tag{17}$$

$$\text{sign}^{\dagger}(\Omega_1, \Omega_2) = \begin{cases} \text{sign}(\Omega_1), & \Omega_1 \neq 0 \\ \text{sign}(\Omega_2), & \Omega_1 = 0. \end{cases} \tag{18}$$

Next, we address a very useful property of the control law above.

Lemma 3.1: The time-optimal control law $u_1^*(t)$ in (16) for (14) is also the optimal control law for the minimum overshoot σ, as defined by (6), i.e., the goal of (9) is also achieved under the same control law. Furthermore, the minimum overshoot equals to

$$\sigma = \max\left(|e_1(0)|, \left|e_1(0) + \frac{\dot{e}_1(0)|\dot{e}_1(0)|}{2b_1\bar{u}_1}\right|\right). \tag{19}$$

Proof: According to the locations of the initial state in the phase plane, as shown in Fig. 4, we divide the right-half plane into three regions indicated by I, II, and III, where the curve going through the point $O(0,0)$ is

$$\dot{e}_1(t) = -\text{sign}(e_1(t))\sqrt{2b_1\bar{u}_1|e_1(t)|}. \tag{20}$$

For the initial states in the left-half plane, it is easy to follow the similar divisions and proof procedure as stated below, which are omitted for simplicity.

Suppose each region contains a sample point A, B, and C, respectively. Applying the time-optimal control law u_1^* (16) to (14), it is straightforward to verify that the state trajectory of $(e_1(t), \dot{e}_1(t))$ is a parabola, which appears as the three cases of curves, as shown in Fig. 4. The curves going upward correspond to $u_1 = \bar{u}_1$, and those going downward correspond to $u_1 = -\bar{u}_1$. The point $O(0,0)$, which is the target state, corresponds to $u_1 = 0$.

To prove the time-optimal control law $u_1^*(t)$ can also achieve the minimum overshoot compared with other control laws, we define $(e_1^*(t), \dot{e}_1^*(t))$ as the state response under u_1^*, while $(e_1(t), \dot{e}_1(t))$ under nonoptimal control law $|u(t)| \leq \bar{u}_1$. In the sequel, we derive the result (19) by proving three cases as follows.

Case 1: When the initial state $x_e(0)$ is in region I, e.g., point $A(e_1(0), \dot{e}_1(0))$ (see Fig. 4), then the state trajectory under u_1^* starts with $u_1 = -\bar{u}_1$ until getting to point A'' and then reaching the target point O by switching $u_1 = \bar{u}_1$. It can be easily observed from Fig. 4 that the overshoot occurs at point $A'(e_1^*(t_1), 0)$, where t_1 denotes the time it takes to travel from point A to A'. Next, we consider the system is under nonoptimal control law $u_1(t)$ within the time interval $t \in [0, t_1]$. Then, we have

$$\begin{cases} \dot{e}_1^*(t) = \dot{e}_1(0) + \int_0^t b_1(-\bar{u}_1)dt, & t \in [0, t_1] \\ \dot{e}_1(t) = \dot{e}_1(0) + \int_0^t b_1 u_1(t)dt, & t \in [0, t_1]. \end{cases} \tag{21}$$

From the above equation, we can obtain

$$\begin{aligned} e_1^*(t) - e_1(t) &= \int_0^t (\dot{e}_1^*(t) - \dot{e}_1(t))dt \\ &= -\int_0^t b_1(u_1(t) + \bar{u}_1)dt \\ &\leq 0, \qquad t \in [0, t_1]. \end{aligned} \tag{22}$$

This implies that the time-optimal control law u_1^* has the minimum overshoot σ. Now, let $e_1^*(t) = 0$ in (21) and we can obtain

$$t_1 = \frac{\dot{e}_1(0)}{b_1\bar{u}_1}.$$

Integrating (21) with the obtained t_1 above, we can calculate the minimum overshoot

$$\sigma = e_1^*(t_1) = e_1(0) + \frac{\dot{e}_1(0)|\dot{e}_1(0)|}{2b_1\bar{u}_1}. \tag{23}$$

Case 2: When the initial state $x_e(0)$ is in region II, e.g., point $B(e_1(0), \dot{e}_1(0))$, then the state trajectory under u_1^* follows the curve $B \to B' \to O$. It can be easily observed from Fig. 4 that the overshoot occurs at point B and thus equals to $e_1(0)$. For nonoptimal control law $u_1(t)$, we can easily obtain

$$e_1^*(t) \leq e_1(0) = \sigma \leq \min_{u_1 \in \mathcal{U}} \max_{t \geq 0} |e_1(t)|. \tag{24}$$

Case 3: When the initial state $x_e(0)$ is in region III, e.g., point $C(e_1(0), \dot{e}_1(0))$, then the state trajectory under u_1^* follows the curve $C \to C' \to C'' \to O$, where point $C'(e_1^*(t_1), 0)$. Then, we have

$$e_1^*(t_1) \leq e_1^*(t) \leq e_1(0) \qquad t \in [0, +\infty). \tag{25}$$

For nonoptimal control law $u_1(t)$ within the time interval $t \in [0, t_1]$, we have

$$e_1^*(t) - e_1(t) \geq 0, \qquad t \in [0, t_1]. \tag{26}$$

It follows that:

$$e_1(t_1) \leq e_1^*(t_1) \leq e_1^*(t) \leq e_1(0) \qquad t \in [0, +\infty). \tag{27}$$

Therefore, we have

$$\begin{aligned} \sigma &= \max\left(|e_1(0)|, |e_1^*(t_1)|\right) \\ &= \max\left(|e_1(0)|, \left|e_1(0) + \frac{\dot{e}_1(0)|\dot{e}_1(0)|}{2b_1\bar{u}_1}\right|\right). \end{aligned} \tag{28}$$

We can easily follow the above procedure to get the results for initial states in the left-hand plane. Combined the results from the different cases, we can finally get the result in (19).

Thus, the proof is completed. □

Remark 3.1: We now prove that using the TOC $u_1^*(t)$ to drive the primary actuator from $x_e(t_2) = [p, -v]$ to $x_e(t_2 + t_r) = [0, 0]$ will lead to the minimum overshoot σ as well. The fact holds if the process is inversed. That is, we can drive the primary actuator from $x_e(t_1) = [0, 0]$ to $x_e(t_1 + t_r) = [p, v]$ by applying $u_1^*(t)$ to achieve the identical performance. Either tracking error trajectory is actually the mirroring of the other. More specifically, we have

$$\min_{u_1 \in \mathcal{U}} \max_{t_1 \le t \le t_1 + t_r} |e_1(t)| = \min_{u_1 \in \mathcal{U}} \max_{t_2 \le t \le t_2 + t_r} |e_1(t)| = \max\left(|p|, \left|p - \frac{v|v|}{2b_1\bar{u}_1}\right|\right). \quad (29)$$

From the above analysis, we shall obviously adopt the TOC $u_1^*(t)$ as the preview control law $u_{1-}(t)$ as will be stated next.

B. Optimal Preview Control

The preview control algorithm can take the advantage of the information of the triangular reference to further reduce the overshoot. The optimal preview control law that can achieve the goals of (9)–(11), is stated as follows.

Lemma 3.2: The optimal preview controller $u_{1-}(t)$ with the following form:

$$u_{1-}(t) = \text{sign}^{\dagger}(\Omega_1, \Omega_2)\bar{u}_1, \qquad t \in \left[-\frac{|v_1 - v_2|}{b_1\bar{u}_1}, 0\right) \quad (30)$$

$$\Omega_1 = -2b_1\bar{u}_1\left(e_1(t) + \text{sign}(v_1 - v_2)\frac{(v_1 - v_2)^2}{16b_1\bar{u}_1}\right) - \left|\dot{e}_1(t) - \frac{v_2 - v_1}{2}\right|\left(\dot{e}_1(t) + \frac{v_2 - v_1}{2}\right)$$

$$\Omega_2 = \frac{v_2 - v_1}{2} - \dot{e}_1(t)$$

can lead to the minimal overshoot

$$\sigma = \frac{|v_1 - v_2|^2}{16b_1\bar{u}_1} \quad (31)$$

where $v_1 = \dot{r}(t)$, $t \in (t_-, 0)$, and $v_2 = \dot{r}(t)$, $t \in (0, t_+)$. Note that the symbols t_- and t_+ are shown in Fig. 2.

Proof: Because the primary actuator output trajectory and velocity is continuous, we have

$$\begin{cases} e_1(0^-) = e_1(0^+) = e_1(0) \\ \dot{e}_1(0^-) = \dot{y}_1(0) - v_1 \\ \dot{e}_1(0^+) = \dot{y}_1(0) - v_2. \end{cases} \quad (32)$$

According to (29), we can obtain

$$\sigma_1 = \max\left(|e_1(0)|, \left|e_1(0) - \frac{\dot{e}_1(0^-)|\dot{e}_1(0^-)|}{2b_1\bar{u}_1}\right|\right) \quad (33)$$

for $-\tau_p \le t \le 0$.

From Lemma 3.1, we can obtain

$$\sigma_2 = \max\left(|e_1(0)|, \left|e_1(0) + \frac{\dot{e}_1(0^+)|\dot{e}_1(0^+)|}{2b_1\bar{u}_1}\right|\right) \quad (34)$$

for $t > 0$.

Therefore, we have

$$\sigma = \max(\sigma_1, \sigma_2) = \max\left(|e_1(0)|, \left|e_1(0) - \frac{(\dot{y}_1(0) - v_1)|\dot{y}_1(0) - v_1|}{2b_1\bar{u}_1}\right|, \left|e_1(0) + \frac{(\dot{y}_1(0) - v_2)|\dot{y}_1(0) - v_2|}{2b_1\bar{u}_1}\right|\right). \quad (35)$$

To simplify the proof, we use the symbols d and v to replace $e_1(0)$ and $\dot{y}_1(0)$, respectively.

Case 1: When $d + \min((v_1 - v)^2/2b_1\bar{u}_1, (v_2 - v)^2/2b_1\bar{u}_1) \ge 0$, and $v_2 < v < v_1$, from (35), we can obtain

$$\sigma = \max\left(|d|, d + \max\left(\frac{(v_1 - v)^2}{2b_1\bar{u}_1}, \frac{(v_2 - v)^2}{2b_1\bar{u}_1}\right)\right) \ge \max\left(|d|, d + \frac{(v_1 - v_2)^2}{8b_1\bar{u}_1}\right) \ge \frac{(v_1 - v_2)^2}{16b_1\bar{u}_1}. \quad (36)$$

Therefore, $\sigma = (v_1 - v_2)^2/16b_1\bar{u}_1$ only when $v = (v_1 + v_2)/2$ and $d = \text{sign}(v_2 - v_1)[(v_1 - v_2)^2/16b_1\bar{u}_1]$.

When $d + \min((v_1 - v)^2/2b_1\bar{u}_1, (v_2 - v)^2/2b_1\bar{u}_1) < 0$ and $v_2 < v < v_1$, it is easy to derive that

$$\sigma > \frac{(v_2 - v)^2}{8b_1\bar{u}_1}. \quad (37)$$

Case 2: When $v \le v_2 < v_1$, from (35), we have

$$\sigma \ge \max\left(|d|, \left|d + \frac{(v_1 - v_2)^2}{2b_1\bar{u}_1}\right|\right) \ge \frac{(v_1 - v_2)^2}{4b_1\bar{u}_1}. \quad (38)$$

Case 3: When $v_2 < v_1 \le v$, it is straightforward to obtain the same result as (38).

When $v_1 < v_2$, we can also obtain $\sigma = (v_1 - v_2)^2/16b_1\bar{u}_1$ only when $\dot{y}_1(0) = (v_1 + v_2)/2$ and $e_1(0) = \text{sign}(v_2 - v_1)[(v_1 - v_2)^2/16b_1\bar{u}_1]$.

The TOC control signals $u_{1-}(t)$, which drive the primary stage from $x_e(-\tau_p) = 0$ to

$$x_e(0^-) = \left[-\text{sign}(v_1 - v_2)\frac{|v_1 - v_2|^2}{16b_1\bar{u}_1}, \quad \frac{v_2 - v_1}{2}\right]$$

can be easily calculated by the traditional time optimal theory. Its form eventually turns out to be that of (30). The derivation process is omitted for simplicity.

Thus, the proof is completed. □

Remark 3.2: Fig. 5 shows the system state trajectory under the preview control law in the case of $v_2 > v_1$, where the system is driven from the origin O to point P' and finally reaches the target point P, the state of which is given by the aforementioned $x_e(0^-)$. The curve going through the point P is the switching curve with $\Omega_1 = 0$. Similar to Fig. 4, the curves going upward correspond to $u_1 = \bar{u}_1$, and those going downward correspond to $u_1 = -\bar{u}_1$.

Remark 3.3: From Lemma 3.2, we can make a constraint on the preview time length τ_p as follows:

$$\tau_p \ge \frac{|v_1 - v_2|}{b_1\bar{u}_1}. \quad (39)$$

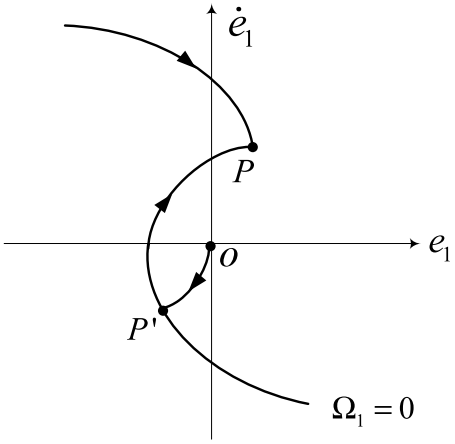

Fig. 5. Illustration of system state trajectory and switching curve under the preview control law.

Remark 3.4: Consider a special case with $v_1 = -v_2 = v_x$, according to (31), we can achieve a minimum overshoot

$$\sigma_{\text{preview}} = \frac{v_x^2}{4b_1\bar{u}_1} \tag{40}$$

under the optimal preview control. To compare with the result without preview (19), we set $e_1(0) = 0$ and $\dot{e}_1(0) = 2v_x$ for a fair comparison. Then, we have

$$\sigma_{\text{nonpreview}} = \frac{2v_x^2}{b_1\bar{u}_1}. \tag{41}$$

It is obvious that the optimal preview control has greatly reduced the overshoot by eight times from that of nonpreview control.

C. Combination With PTOS for Practical Implementation

For practical implementation and robustness, we use the PTOS controller [23] to approximate the postactuated time-optimal control law u_{1+}. Its control law is given by

$$u_{1+} = \text{sat}[k_2(-f(e_1) - \dot{y}_1 + \dot{r})] \tag{42}$$

where

$$f(e_1) = \begin{cases} \frac{k_1}{k_2}e_1, & \text{for } |e_1| \le y_l \\ \text{sign}(e_1)\left(\sqrt{2b_1\bar{u}_1|e_1|} - \frac{\bar{u}_1}{k_2}\right), & \text{for } |e_1| > y_l \end{cases} \tag{43}$$

where sat$[\cdot]$ is with the saturation level of $\bar{u}_1$, k_1, and k_2 are constant gains, which can be designed by traditional pole-placement method [23]. $\dot{r}(t)$ is the derivative of $r(t)$ with the convention that $\dot{r}(t) = 0$ at the turning points of $r(t)$. The following constraints guarantee a continuous switching of the controller:

$$y_l = \frac{\bar{u}_1}{k_1}, \quad k_2 = \sqrt{\frac{2k_1}{b_1}} \tag{44}$$

where y_l is the linear region close to the setpoint, which is introduced to reduce the control chatter.

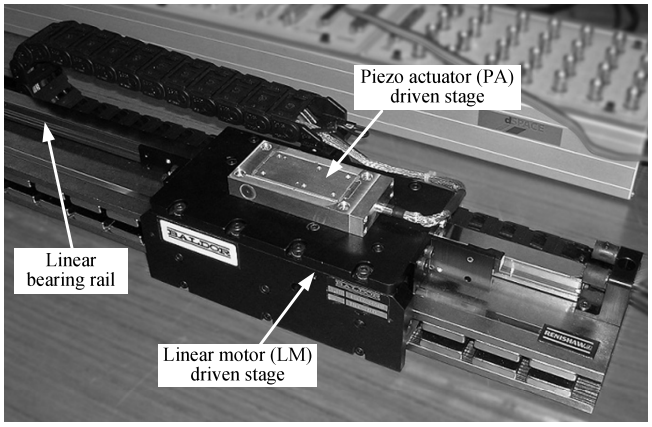

Fig. 6. Experimental setup of the DSA positioner.

IV. Secondary Actuator Control Design

To complete the task of compensating for the primary actuator tracking error, the secondary actuator controller is designed as a linear feedback-feedforward controller borrowed from [19] with a trivial modification. Its control law is given by

$$u_2 = u_{2L} + u_{2F} \tag{45}$$

where u_{2L} is a linear feedback control law with

$$u_{2L} = [w_1 \;\; w_2]x_2 \tag{46}$$

where w_1 and w_2 can be calculated by the linear control design method as proposed in [19] to achieve an appropriate bandwidth and damping ratio for the secondary actuator. The feedforward control signal u_{2F} is given by

$$u_{2F} = \frac{1}{b_2}((a_1 + b_2w_1)e_1 + (a_2 + b_2w_2)\dot{e}_1 - b_1u_1) \tag{47}$$

which leads to the design objective $y_2 = -e_1$. This can be easily verified by substituting (45) into the secondary actuator plant model in (2) and by applying the fact of $b_1u_1 = \ddot{y}_1 = \ddot{e}_1$.

With the primary actuator controller in (30) and (42) and the secondary actuator controller given by (45), we can simply follow the proof in [19, Lemma 1] to obtain the result that the total tracking error of the DSA system will asymptotically converge to zero for any triangular reference even in the presence of actuator saturation.

V. Experimental Results

This section carries out the experiments to study the proposed control design. The experimental setup is shown in Fig. 6, which consists of a LM with a 500 cm travel range and a piggyback PA with a ± 15 μm travel range. The LM position is measurable by a 1-μm resolution optical encoder and the PA position relative to the LM can be detected by a capacitive sensor with 0.2-nm resolution. Because the total dual-stage position output is the summation of the positions between the LM and the PA, the ideally best dual-stage positioning accuracy is thus limited by the resolution of the LM encoder, i.e., 1 μm. In reality, the system contains several undesired

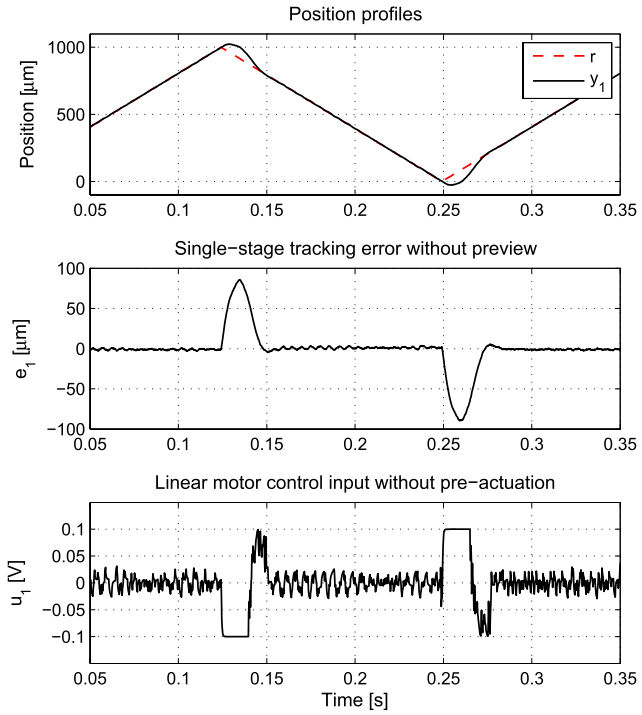

Fig. 7. Single-stage (with LM only) tracking control without preview. The maximum tracking error is 88 μm.

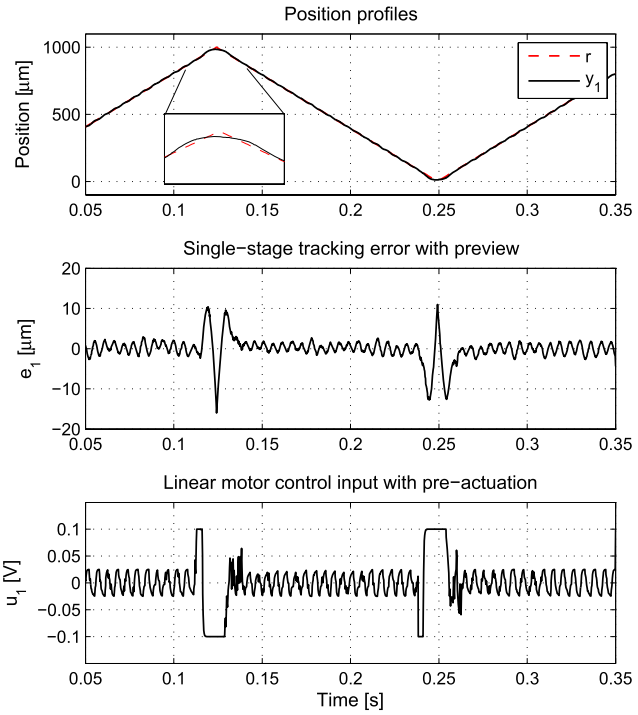

Fig. 8. Single-stage (with LM only) tracking control with preview. The maximum tracking error is significantly reduced to 15 μm due to the optimal preview control.

dynamics such as the nonlinear friction in the LM and the hysteresis effect and resonance mode in the PA. To shape the system model equivalent to (2), we employ an inner-loop fast servo controller to eliminate these undesired dynamics [19]. Therefore, the resultant DSA model parameters are given as follows:

$$b_1 = 1.5 \times 10^7, \quad \bar{u}_1 = 0.1 \text{ V}$$
$$b_2 = 3 \times 10^6, \quad a_1 = -10^6, \quad a_2 = -1810$$
$$\bar{u}_2 = 5 \text{ V}, \quad \bar{y}_2 = 15 \ \mu\text{m}.$$

The triangular reference for the control validation is chosen with the period of $T = 0.2$ s and the amplitude of 1000 μm. We follow the proposed controller design to obtain the control parameters as follows:

$$k_1 = 0.0095, \quad k_2 = 4.78 \times 10^{-5}$$
$$w_1 = -0.8385, \quad w_2 = -0.0005$$

and according to (30), the preview time length $\tau_p = 0.0107$ second. The controllers were implemented by a real-time DSP system (dSPACE-DS1103) with the sampling frequency of 5 kHz. The velocities of the LM and PA stage are estimated by the backward differentiation of the feedback position signals, respectively.

A. Single-Stage Actuator Tracking Results

First, we perform single-stage tracking control with the LM only to validate the efficacy of the preview controller. Fig. 7 shows the experimental results. We can observe that the maximum tracking error is 88 μm. When the preview controller is applied, the maximum tracking error is greatly reduced to 15 μm, as shown in Fig. 8. Moreover, this result closely matches the theoretical value (i.e., 13 μm) according to the formula, as derived in (31). From the top plot of Fig. 8, the zoomed-in position profiles clearly imply the reason why the optimal preview control strategy can effectively minimize the overshoot is because an equivalent amount of undershoot is introduced at the turning point of the triangular reference.

Note that the time responses of e_1 and u_1 during steady state, as shown in Figs. 7 and 8 contain some oscillations. This is mainly caused by the encoder quantization noise and the velocity estimation error, which are difficult to eliminate completely. However, we observe that the positioning accuracy in steady state achieved is within ± 2 μm, which is actually closed to the ideal performance as compared with the encoder resolution aforementioned.

B. DSA Tracking Results

Next, we apply the optimal preview controller to the LM together with the PA controller, which is used to compensate for the LM tracking error. Fig. 9 shows that the maximum tracking error achieved by the DSA without preview is 73 μm, which, however, cannot be further reduced because the LM tracking error is beyond the PA travel range, as shown in Fig. 7. Finally, Fig. 10 shows the DSA tracking control with preview, which shows that the maximum tracking error is significantly reduced to 5 μm. Moreover, the settling time (defined by the time it takes for the tracking error to converge within ± 2 μm) achieved is only 0.005 s, which is much smaller than 0.021 s achieved by the case without preview, as shown in Fig. 9.

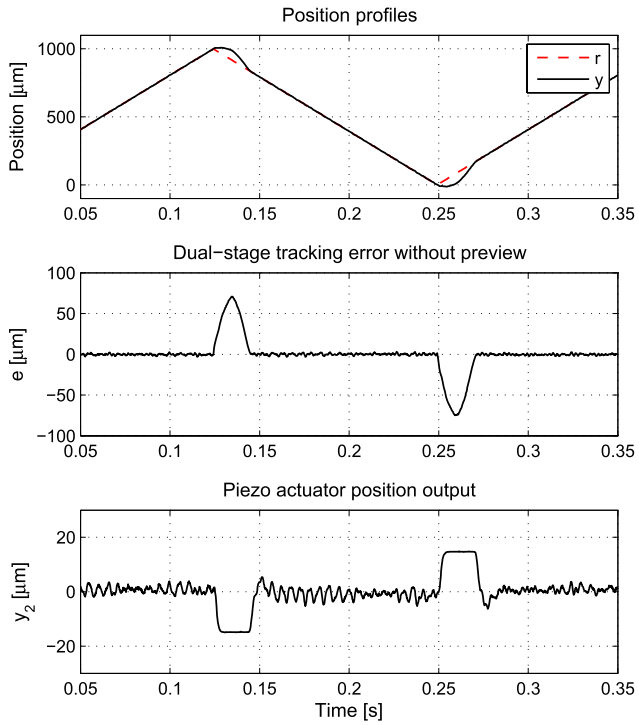

Fig. 9. Dual-stage tracking control without preview. The maximum tracking error with the use of the PA is 73 μm but cannot be further reduced because the maximum tracking error generated by the LM without preview control is beyond the PA travel range, as shown in Fig. 7.

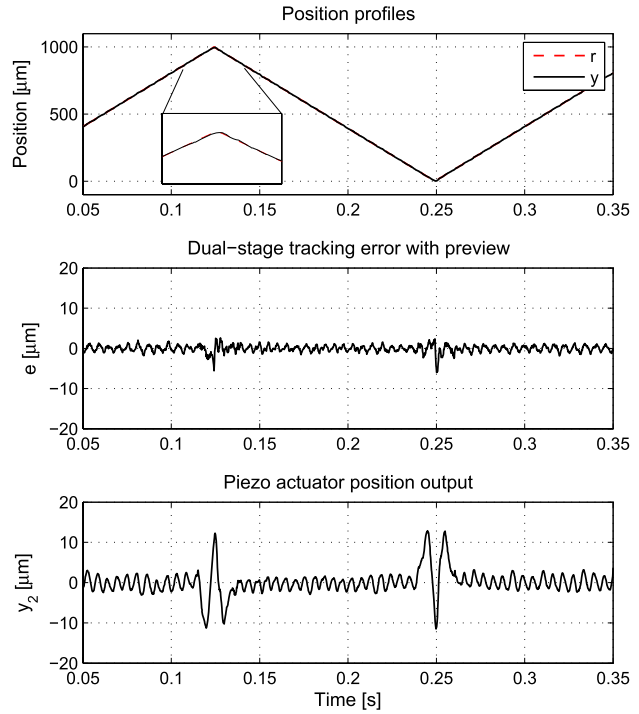

Fig. 10. Dual-stage tracking control with preview. The maximum tracking error is further reduced from 15 μm (see single-stage preview control in Fig. 8) to 5 μm by the PA. Moreover, the settling time is reduced to 0.005 s as compared with the case of 0.021 s without preview (see Fig. 9).

Finally, the implementation results of the above experiments are summarized in Table I for easy comparison. It is shown that compared with the nonpreview cases the proposed optimal preview control can reduce the settling time by more than 50% and the maximum tracking error by at least five times in either the single-stage control or the dual-stage control. These results coincide with our theoretical analysis. Hence, the experimental results confirm that the proposed optimal preview controller can achieve accurate triangular reference tracking performance not only with a minimal settling time but also with a minimal overshoot for the DSA system.

TABLE I
COMPARISON OF THE TRACKING PERFORMANCE

Compared Experiments	Settling Time (ms)	Maximum Tracking Error (μm)
Single-stage w/o preview	32	88
Single-stage w/ preview	13	15
Dual-stage w/o preview	21	73
Dual-stage w/ preview	5	5

VI. CONCLUSION

In this brief, we have proposed an optimal preview control law with the use of the information of the future references for a class of DSA systems to track triangular references fast and accurately. It is proved that the optimal preview control can not only reduce the settling time, but also minimize the overshoot of the primary stage, which beneficially leads to a reference profile of minimal amplitude for the secondary stage to compensate and also minimizes the control effort of the secondary actuator as a result. Experimental results on a real DSA positioning system are shown to verify the effectiveness of the proposed optimal preview control design and its feasible application on the dual-stage control systems.

REFERENCES

[1] K. Mori, T. Munemoto, H. Otsuki, Y. Yamaguchi, and K. Akagi, "A dual-stage magnetic disk drive actuator using a piezoelectric device for a high track density," *IEEE Trans. Magn.*, vol. 27, no. 6, pp. 5298–5300, Nov. 1991.

[2] T. Gao, C. Du, C. P. Tan, Z. He, J. Yang, and L. Xie, "High bandwidth control design and implementation for a dual-stage actuation system with a micro thermal actuator," *IEEE Trans. Magn.*, vol. 49, no. 3, pp. 1082–1087, Mar. 2013.

[3] T. Hirano, H. Takahashi, S. Hagiya, N. Nishiyama, and T. Tsuchiya, "High bandwidth micro electro mechanical systems (MEMS) microactuator for hard-disk drive dual-stage tracking servo," in *Proc. ASME Annu. Conf. Inf. Storage Process. Syst.*, 2010, pp. 1–12.

[4] B.-S. Kim, J. Li, and T.-S. Tsao, "Two-parameter robust repetitive control with application to a novel dual-stage actuator for noncircular machining," *IEEE/ASME Trans. Mechatron.*, vol. 9, no. 4, pp. 644–652, Dec. 2004.

[5] S. J. Kwon, W. K. Chung, and Y. Youm, "On the coarse/fine dual-stage manipulators with robust perturbation compensator," in *Proc. IEEE Int. Conf. Robot. Autom.*, Jan. 2001, pp. 121–126.

[6] J. Zheng, A. Salton, and M. Fu, "Design and control of a rotary dual-stage actuator positioning system," *Mechatronics*, vol. 21, pp. 1003–1012, Sep. 2011.

[7] A. T. Elfizy, G. M. Bone, and M. A. Elbestawi, "Design and control of a dual-stage feed drive," *Int. J. Mach. Tools Manuf.*, vol. 45, pp. 153–165, Jan. 2005.

[8] S. J. Schroeck, W. C. Messner, and R. J. McNab, "On compensator design for linear time-invariant dual-input single-output systems," *IEEE/ASME Trans. Mechatron.*, vol. 6, no. 1, pp. 50–57, Mar. 2001.

[9] J. Zheng and M. Fu, "A unified dual-stage actuator control scheme for track seeking and following in hard disk drives," *IET Control Theory Appl.*, vol. 6, no. 10, pp. 1468–1477, Feb. 2012.
[10] J. Zheng, M. Fu, C. Du, Y. Wang, and L. Xie, "A factorization approach to sensitivity loop shaping for disturbance rejection in hard disk drives," *IEEE Trans. Magn.*, vol. 46, no. 5, pp. 1220–1227, May 2010.
[11] G. Herrmann, M. C. Turner, I. Postlethwaite, and G. Guo, "Practical implementation of a novel anti-windup scheme in a HDD-dual-stage servo system," *IEEE/ASME Trans. Mechatron.*, vol. 9, no. 3, pp. 580–592, Sep. 2004.
[12] T. Shen and M. Fu, "High precision and feedback control design for dual-actuator systems," in *Proc. IEEE Conf. Control Appl.*, Aug. 2005, pp. 956–961.
[13] D. Kim, K.-T. Nam, S. H. Ji, and S. M. Lee, "Modeling of a dual actuator system and its control algorithm preventing saturation of fine actuator," in *Proc. IEEE/ASME Int. Conf. Adv. Intell. Mechatron.*, Jul. 2011, pp. 530–535.
[14] G. Whitesides and H. Love, "The art of building small," *Sci. Amer.*, vol. 285, no. 3, pp. 39–47, Sep. 2001.
[15] J. Yi, S. Chang, and T. Shen, "Disturbance-observer-based hysteresis compensation for piezoelectric actuators," *IEEE/ASME Trans. Mechatron.*, vol. 14, no. 4, pp. 456–464, Aug. 2009.
[16] D. Abramovitch, S. Andersson, L. Pao, and G. Schitter, "A tutorial on the mechanisms, dynamics, and control of atomic force microscopes," in *Proc. Amer. Control Conf.*, 2007, pp. 3488–2208.
[17] A. Fleming, "Nanopositioning system with force feedback for high-performance tracking and vibration control," *IEEE/ASME Trans. Mechatron.*, vol. 15, no. 3, pp. 433–447, Jun. 2010.
[18] M. Kobayashi, and R. Horowitz, "Track seek control for hard disk dual-stage servo systems," *IEEE Trans. Magn.*, vol. 37, no. 2, pp. 949–954, Mar. 2001.
[19] J. Zheng and M. Fu, "Nonlinear feedback control of a dual-stage actuator system for reduced settling time," *IEEE Trans. Control Syst. Technol.*, vol. 16, no. 4, pp. 717–725, Jul. 2008.
[20] Q. Zou and S. Devasia, "Precision preview-based stable-inversion for nonlinear nonminimum-phase systems: The VTOL example," *Automatica*, vol. 43, no. 1, pp. 117–127, Jan. 2007.
[21] A. Hazell and D. Limebeer, "An efficient algorithm for discrete-time H_∞ preview control," *Automatica*, vol. 44, no. 9, pp. 2441–2448, Sep. 2008.
[22] K. Takaba, "A tutorial on preview control systems," in *Proc. SICE Annu. Conf.*, 2003, pp. 1388–1393.
[23] G. F. Franklin, J. D. Powell, and M. Workman, *Digital Control of Dynamic Systems*, 3rd ed. Reading, MA, USA: Addison Wesley, 1997.